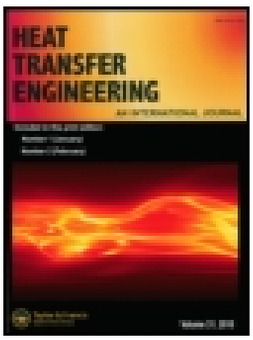

Heat Transfer Engineering

ISSN: 0145-7632 (Print) 1521-0537 (Online) Journal homepage: http://www.tandfonline.com/loi/uhte20

Ultrafast Electron–Phonon Coupling at Metal-Dielectric Interface

Qiaomu Yao, Liang Guo, Vasudevan Iyer & Xianfan Xu

To cite this article: Qiaomu Yao, Liang Guo, Vasudevan Iyer & Xianfan Xu (2018): Ultrafast Electron–Phonon Coupling at Metal-Dielectric Interface, Heat Transfer Engineering, DOI: 10.1080/01457632.2018.1457281

To link to this article: https://doi.org/10.1080/01457632.2018.1457281

Accepted author version posted online: 26 Mar 2018.
Published online: 10 Apr 2018.

HEAT TRANSFER ENGINEERING
2018, VOL. 0, NO. 0, 1–9
https://doi.org/10.1080/01457632.2018.1457281

Taylor & Francis
Taylor & Francis Group

Ultrafast Electron–Phonon Coupling at Metal-Dielectric Interface

Qiaomu Yao, Liang Guo, Vasudevan Iyer, and Xianfan Xu

School of Mechanical Engineering, Birck Nanotechnology Center, Purdue University, West Lafayette, Indiana, USA

ABSTRACT

Energy transfer from photo-excited electrons in a metal thin film to the dielectric substrate is important for understanding the ultrafast heat transfer process across the two materials. Substantial research has been conducted to investigate heat transfer in a metal-dielectric structure. In this work, a two-temperature model in metal was used to analyze the interface electron and dielectric substrate coupling. An improved temperature and wavelength-dependent Drude–Lorentz model was implemented to interpret the signals obtained in optical measurements. Ultrafast pump-and-probe measurements on Au-Si samples were carried out, where the probe photon energy was chosen to be close to the interband transition threshold of gold to minimize the influence of non-equilibrium electrons on the optical response and maximize the thermal modulation to the optical reflectance. Electron-substrate interface thermal conductance at different pump laser fluences was obtained, and was found to increase with the interface temperature.

Introduction

Electron–phonon coupling in metals [1], semiconductors [2], and across metal-dielectric interfaces is an important phenomenon in ultrafast heat transfer experiments. When an ultrafast laser beam is focused on a metal, the photon energy is absorbed first by free electrons, and it takes a few tens to a few hundreds of femtoseconds for electrons to reach thermal equilibrium. The electron–phonon energy coupling also heats up the lattice of the metal. For thin metal films on a dielectric substrate, there can be electron–phonon coupling across the metal-dielectric interface as well, which spreads the energy into the substrate through heat diffusion. Much work have been carried out to quantify the electron–phonon coupling, characterized by a coupling factor G, particularly in gold. For example, Holfeld, et al. [1] found G is independent of the electron temperature in 10 nm–100 nm gold films and is independent of the film thickness within a 20% uncertainty. Other investigations considered the electron–phonon coupling factor G as film thickness and/or pump fluence dependent, and fitted the value of G to the measured thermal reflectance variation [3]–[5]. During the electron relaxation process after the laser irradiation, the excited electrons relax to the Fermi–Dirac distribution mainly through electron–electron collisions and electron–phonon scattering [6]. This thermalization process of excited electrons can influence the optical response, which can be manifested by varying the probe wavelength. Sun et al. [7] found that the optical response is largely influenced by the non-thermalized electrons when probing with wavelengths far from the inter-band transition threshold (ITT, 2.47 eV for gold), but the non-thermalized electrons contributed much less to the optical response at probe energy close to ITT. Guo and Xu [8] confirmed the probe wavelength-dependent optical responses in gold. They used a probe of 490 nm wavelength (2.53 eV), slightly above the ITT of gold, and found the electron–phonon coupling G in gold to be 1.5×10^{16} W/(m^{3}K), which is less than values using other probe wavelengths. A recent study showed the electron–phonon coupling factor G was less influenced by non-thermalized electrons at high pump fluences (up to 10.7 J/m^2) because of the higher rate of electron–electron scattering [9]. Energy coupling between electrons and phonons across interface has also been studied, and a linear relation between the electron–phonon interfacial thermal conductance and the electron temperature was found in Au films using both 800 nm as pump and probe wavelengths [10].

This work investigates interface electron–phonon coupling across the gold-silicon interface. Electron and lattice temperatures in gold together with the lattice temperature

CONTACT Professor Xianfan Xu xxu@ecn.purdue.edu School of Mechanical Engineering, Birck Nanotechnology Center, 1205 West State Street, West Lafayette, Indiana, USA 47907-1288.
Color versions of one or more of the figures in this paper can be found online at www.tandfonline.com/uhte.

in silicon are modeled to account for the electron–phonon coupling in gold and across the interface. The optical response is computed using a modified temperature-dependent Drude–Lorentz model. The probe photon energy is chosen as 2.53 eV to minimize the effect of non-thermalized electrons on the optical response and maximize the effect of thermal modulation. The temperature-dependent electron–phonon coupling factor G is first obtained from the experimental data on bulk gold. This coupling factor is assumed independent of the thin film thickness, and is used to find the temperature-dependent interface resistance or conductance based on the experimental data on gold thin films.

Ultrafast optical measurements

We first discuss the transient reflectivity signals obtained in the pump-and-probe experiments and their dependence on the probe wavelength in gold. Gold has been widely used as the temperature transducer in the studies of ultrafast heat transfer. During femtosecond pump-probe experiments, the laser pulses interact with gold with the following steps [1]: at the time when the pump pulse hits the gold surface, some of the electrons absorb photons. These excited electrons can move into the material ballistically without interacting with the lattice. The initially photo-excited electrons are not in thermal equilibrium. The collisions among these thermally non-equilibrium electrons and with the un-excited electrons form an equilibrium Fermi–Dirac distribution, typically within 10 s to 100 s of femtoseconds. This equilibrium state can then be represented using an electron temperature. Through the electron–phonon coupling process, the electron temperature will decrease and the lattice temperature will increase. This electron–phonon interaction typically takes several picoseconds until electrons and phonons reach thermal equilibrium.

The optical response resulting from the energy transfer process described above can be explained by the band structure of gold. Gold has a typical band structure as a noble metal. The free electrons in the *s/p* band follow the Fermi–Dirac distribution [6]:

$$f\ (E, T) = \frac{1}{e^{(E-E_f)/k_B T} + 1} \tag{1}$$

where E denotes the energy, E_f is Fermi energy of gold, k_B is Boltzmann constant, and T is absolute electron temperature. Due to the variation of electron occupancy with temperature, both the *d* band and *s/p* band excitation will affect the absorption of light and cause the change in optical response. Figure 1 shows the electron occupancy of gold and the Fermi–Dirac distribution near the Fermi energy, which can explain the impact of the change of the Fermi–Dirac distribution on the optical reflectance.

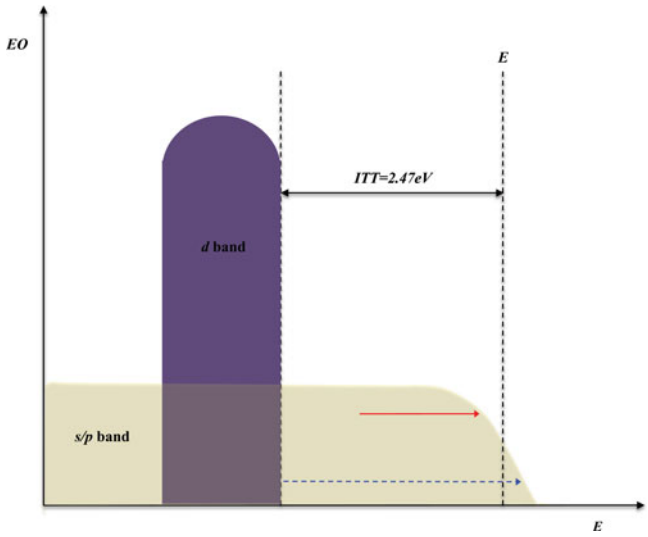

Figure 1. Interband transition from d band to *s/p* band (dashed arrow) and intraband transition inside *s/p* band (solid arrow) in gold, where gold has an ITT of 2.47 eV. The vertical axis represents the electron occupation (EO). The electrons in *s/p* band follow the Fermi–Dirac distribution.

As the temperature increases, the occupation of electrons with energy above the Fermi energy increases and the occupation of electrons with energy below the Fermi energy decreases. For probe photon energy larger than ITT (as indicated by the dashed arrow in Figure 1), the change in the electron distribution will decrease the photon absorption for electron transitions from the *d* band to unfilled energy states above the Fermi energy and thus increase the reflection. On the other hand, for probe photon energy less than ITT, the absorption increases and the reflection decreases. These trends were experimentally observed [2], [8].

Non-thermalized electrons do not follow the Fermi–Dirac distribution and do not have a well-defined temperature, so the two-temperature model (TTM) does not apply. Del Fatti et al. [11] experimentally determined that these non-thermalized electrons exist for the first few hundred femtoseconds after the laser pulse. Guo and Xu [8] obtained the probe wavelength-dependent transient reflectance and showed the relative contribution from the non-thermalized electrons to the transient reflectance signal. The thermalized electron distribution vs. non-thermalized electron distribution is shown in Figure 2 (adopted from [8] for its importance). It is seen that when the probed state is far from the Fermi energy, the optical signal will be mainly caused by the non-thermalized electrons. In order to minimize the effect of the non-thermalized electrons on the transient reflectance change, the 490 nm probe wavelength (2.53 eV) is chosen in this work for the measurements for which the influence from thermalized electrons is much larger than non-thermalized electrons.

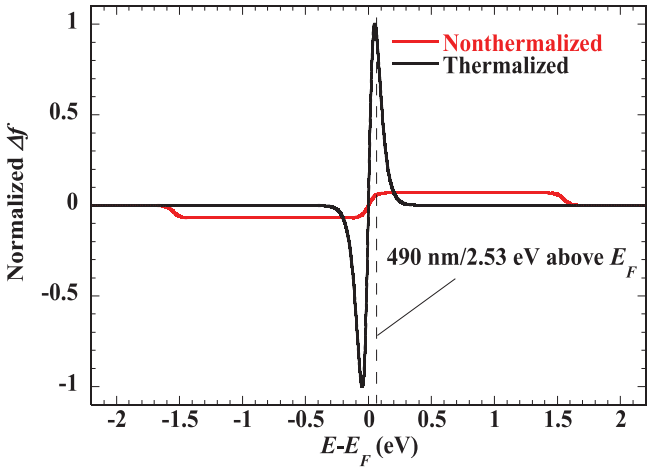

Figure 2. Electron distribution change for non-thermalized electrons and thermalized electrons created by an 800 nm pulse, the dashed line indicates the detected state by the probe energy of 2.53 eV (490 nm) and therefore the change from non-thermalized electrons is much less than that from thermalized electrons (adopted from [8]).

Experiment configuration

A Ti-Sapphire amplified femtosecond laser is used to generate laser pulses with 100 fs pulse width, central wavelength at 800 nm, and repetition rate of 5 kHz. A collinear pump and probe technique is used by dividing the laser beam into a relatively weak probe beam and higher power pump beam. The pump beam is focused to a 29.8 μm radius on the sample. The probe beam is sent to an optical parametric amplifier (OPA), which generates tunable wavelengths with nonlinear processes. The output from the OPA is fixed at the 490 nm wavelength in order to reduce the effect of non-thermalized electrons as discussed above. The probe spot radius is 13.8 μm, smaller than half of the pump spot radius. A computer-controlled mechanical delay stage is used to adjust the time delay between the pump and the probe beams in femtosecond time step.

Gold films were deposited on silicon substrates using electron beam evaporation. The substrates were cleaned using toluene, acetone, methanol, and isopropanol before the gold deposition. Thin gold films with thicknesses of 24 nm, 39 nm, and 65 nm, and bulk gold (>1 μm thick gold film on silicon) are measured at varying pump fluences. The bulk gold sample is used to identify the interface-independent factors such as the electron–phonon coupling within the gold film, and helps to distinguish thermal conductance across the interface and the electron–phonon coupling within the films. The oxide layer that develops over the silicon substrate is extremely thin and electrons are assumed to tunnel through this layer and couple with the silicon phonons.

Numerical models

The two-temperature metal-dielectric interface model

The interaction between electrons and phonons, when there exists thermal non-equilibrium between electrons and phonons within the metal, can be described by the TTM [12]–[14]:

$$C_e \frac{\partial T_e}{\partial t} = k_e \frac{\partial^2 T_e}{\partial x^2} - G(T_e - T_p) + S \tag{2a}$$

$$C_p \frac{\partial T_p}{\partial t} = k_p \frac{\partial^2 T_p}{\partial x^2} + G(T_e - T_p) \tag{2b}$$

$$C_s \frac{\partial T_s}{\partial t} = k_s \frac{\partial^2 T_s}{\partial x^2} \tag{2c}$$

With interface conditions [15]:

$$-k_e \frac{\partial T_e}{\partial x}\bigg|_{x=L} = \frac{T_e - T_s}{R_{es}}\bigg|_{x=L} \tag{3a}$$

$$-k_p \frac{\partial T_p}{\partial x}\bigg|_{x=L} = \frac{T_p - T_s}{R_{ps}}\bigg|_{x=L} \tag{3b}$$

$$-k_s \frac{\partial T_s}{\partial x}\bigg|_{x=L} = \frac{T_e - T_s}{R_{es}}\bigg|_{x=L} + \frac{T_p - T_s}{R_{ps}}\bigg|_{x=L} \tag{3c}$$

The subscripts e, p, and s stand for electrons, phonons and substrate, respectively. R is the thermal resistance between interfaces. C_e and C_p are the respective heat capacities of electrons and lattice and k_e, k_p denote the thermal conductivity of electrons and phonons. With this formulation, the interaction between electrons and phonons in gold is represented using the coupling factor G, while the possible interaction between electrons in thin films with phonons in the substrate is accounted for in the interface energy transport, Eq. (3a). Hence, G is treated as independent of the film thickness.

The laser source term S is given as [16]:

$$S = 0.94 \frac{1-R}{(\delta + \delta_b)\left(1 - e^{-L/(\delta+\delta_b)}\right)} \cdot \frac{J}{t_p} \exp\left[\frac{-x}{\delta + \delta_b} - 2.77\left(\frac{t}{t_p}\right)^2\right] \tag{4}$$

This equation represents a temporal Gaussian pulse with the consideration of the ballistic motion of electrons and thermal absorption in the x-direction. t_p is the full width at half maximum of the laser pulse, R is the reflectivity of gold film at the pump wavelength calculated using the multilayer approach, L denotes the thickness of sample, δ_b is the ballistic range of electrons which is taken as 100 nm [16], J is the fluence of laser beam, and δ is the optical absorption depth.

The Drude–Lorentz model for optical responses

As discussed earlier, a close to ITT probe beam with a wavelength of 490 nm is used in order to minimize the effects from the non-thermalized electrons. The Drude model combined with Lorentz oscillators is needed to describe the interband transition in metal, and is implemented here to describe the relation among the electron temperature, the phonon temperature, and the probe wavelength with the temperature dependent dielectric function and the resulting temperature dependent reflectance. Earlier studies applied only the Drude model to bridge TTM with reflectance signals [5], [10], [15] where 800 nm probe photon energy was used for intraband transition of electrons. It should be noted that interband transition could happen even with the probe energy less than ITT to states below the Fermi energy, where holes are formed in the *s/p* band due to excitations of these states to higher states.

The combined Drude–Lorentz model for gold considers two Lorentz oscillators at 330 nm and 470 nm to produce a close agreement with the dielectric constant at room temperature [17]. This model is expressed as:

$$\varepsilon = \varepsilon_\infty - \frac{\omega_p^2}{\omega(\omega + i\Gamma_0)} + L_1(\omega) + L_2(\omega) \tag{5}$$

where the first two terms are the contributions of the Drude model. L_1 and L_2 are the Lorentz oscillators that describe the contributions of interband transitions. ε_∞ is the high frequency limit of dielectric constant, Γ_0 is the Drude damping term which stands for the scattering rate of free electrons, ω_p is the plasma frequency (1.37×10^{16} rad/s in Au [6]). The two interband transition terms are expressed as [17]:

$$L_i(\omega) = D_i\left[e^{i\phi_i}(\omega_i - \omega - i\Gamma_i)^{\mu_i} + e^{-i\phi_i}(\omega_i + \omega + i\Gamma_i)^{\mu_i}\right] \tag{6}$$

D_i is the amplitude for the oscillator, ω_i is the resonant frequency, ϕ_i is the phase, μ_i is the order of pole, which is used to characterize the dielectric constant involving several close transitions (-1 for both transitions of gold), and Γ_i is the damping factor. This model has proven to be consistent with the Kramers–Kronig relation [17], [18].

The damping factor can be described as a result of electron–electron scattering and electron–phonon scattering and is expressed as [6], [15], [19]:

$$\Gamma_i = A_{eei}T_e^2 + B_{epi}T_p + Y_i \tag{7}$$

The subscripts i are 0, 1, and 2 for the Drude term and the two Lorentz terms, respectively. For the damping factor in the Drude model Γ_0, the coefficient describing electron–electron scattering A_{ee0} is taken as 1.2×10^7 $s^{-1}K^{-2}$ which is obtained from the low temperature Fermi liquid theory [20]. B_{ep0} is chosen as 3.6×10^{11} $s^{-1}K^{-1}$ which is predicted by matching the experimental results of dielectric constant at room temperature [21]. The electron–electron scattering rate of Lorentzian oscillators A_{ee1}, A_{ee2} are assumed to be the same as those in the Drude model A_{ee0}. B_{ep1}, B_{ep2} are determined using room temperature optical constants with Eq. (7) [17]. We also found that a temperature-independent term Y_i needs to be included for the Lorentzian oscillators (Y_0 is taken to be 0), in order to fit the entire optical response. Y_1, Y_2 are found to be 7.9×10^{14} rad/s and 1.9×10^{15} rad/s, respectively. All the parameters are listed in Table 1.

The calculated dielectric constant ($\varepsilon = \varepsilon_1 + i\varepsilon_2$) at room temperature matches with what is given in [17], and this model also provides a temperature- and wavelength-dependent dielectric constant as shown in Figure 3. A closer examination of the difference between the dielectric constant at elevated temperaures and room temperature shows that the change of the real part of dielectric constant ε_1 at 490 nm is more significant compared with those at the neighboring wavelengths (Figure 3a). Thus, the transient reflectance is largely influenced by the real part of the dielectric constant ε_1. The reflectivity is calculated from the dielectric function as [22]:

$$R = \frac{|\varepsilon| - \sqrt{2(\varepsilon_1 + |\varepsilon|)} + 1}{|\varepsilon| + \sqrt{2(\varepsilon_1 + |\varepsilon|)} + 1} \tag{8a}$$

$$|\varepsilon|^2 = \varepsilon_1^2 + \varepsilon_2^2 \tag{8b}$$

The depth-dependent temperature of the film and hence the depth-dependent dielectric constant is taken into account using the multilayer approach. A larger variation of the reflectivity at 490 nm than the neighboring wavelengths was observed in [8]. Thus, using the probe wavelength near ITT not only minimizes the effect of non-thermalized electrons, but also provides the largest optical response for improving the signal-to-noise ratio.

The electron–phonon coupling factor G is regarded as temperature dependent. Its relation with A_{ee0} and B_{ep0} in the Drude model can be expressed as [23]:

$$G(T) = G_0\left(\frac{Aee0}{Bep0}(T_e + T_p) + 1\right) \tag{9}$$

Table 1. Summary of the parameters in the Drude–Lorentz model.

	Value	Parameter (units)	Value
A_{ee0}, A_{ee1}, A_{ee2} ($s^{-1}K^{-2}$)	1.2×10^7	Y_0 (rad/s)	0
B_{ep0} ($s^{-1}K^{-1}$)	3.6×10^{11}	Y_1 (rad/s)	7.9×10^{14}
B_{ep1} ($s^{-1}K^{-1}$)	7.8×10^{10}	Y_2 (rad/s)	1.9×10^{15}
B_{ep2} ($s^{-1}K^{-1}$)	1.9×10^{11}	D_1 (m^{-1})	2.0×10^6
ϕ_1, ϕ_2 (rad)	$-\pi/4$	D_2 (m^{-1})	4.1×10^6
Γ_0 (rad/s)	1.3×10^{16}	μ_1, μ_2 (rad)	-1
ε_∞	1.53	ω_1 (rad/s)	4.0×10^{15}
ω_p (rad/s)	1.37×10^{16}	ω_2 (rad/s)	5.7×10^{15}

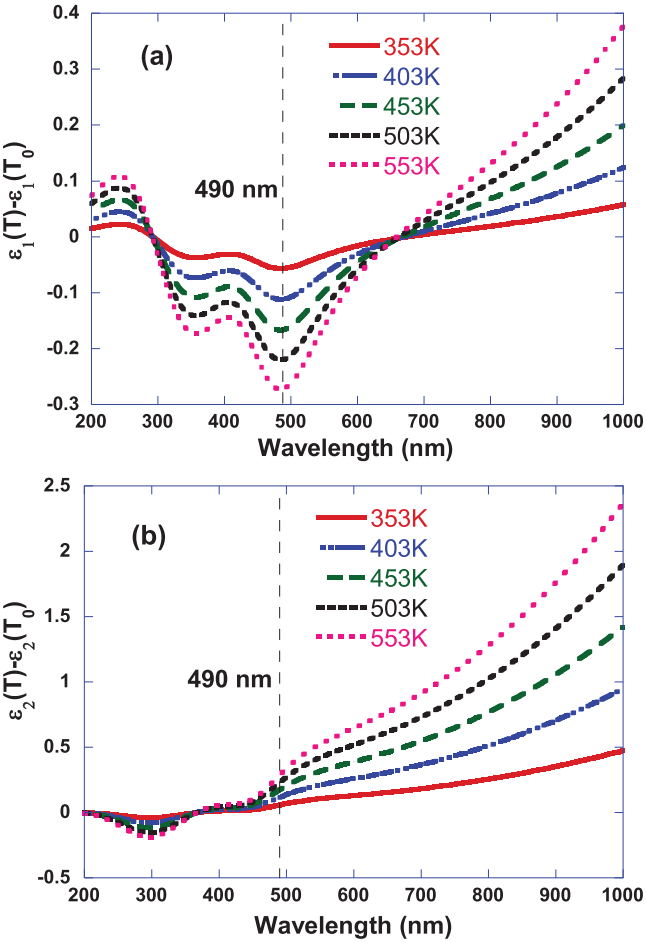

Figure 3. Calculated real part (3a) and imaginary part (3b) of dielectric constant ε_1 and ε_2 vs. wavelength and temperature using the Drude–Lorentz model.

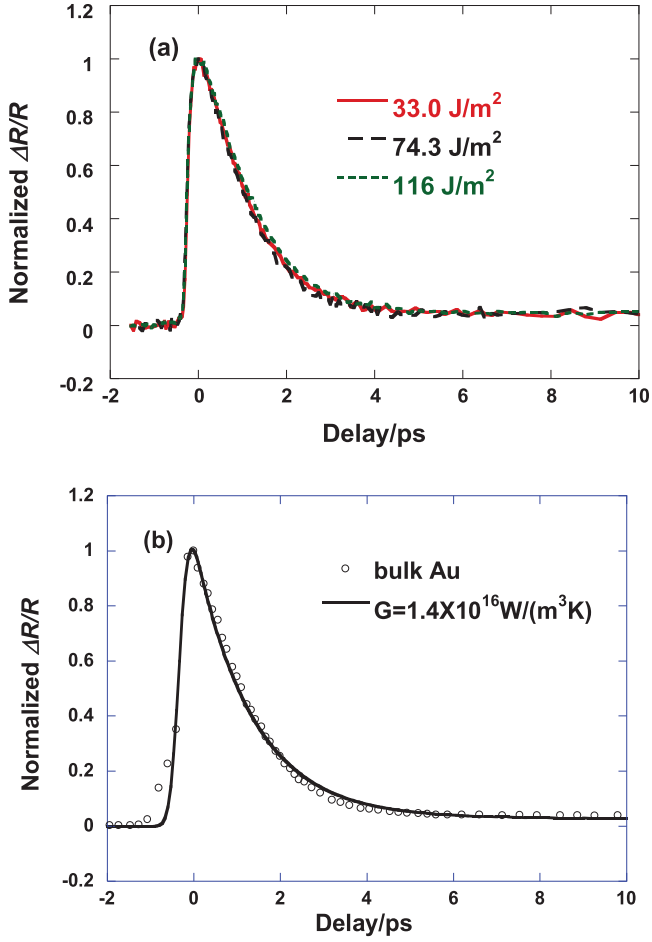

Figure 4. (a) Experiment result of bulk gold using 490 nm probe and 800 nm pump with pump fluence at 33.0, 74.3, and 116 J/m^2. (b) Fitting result of bulk Au at 33.0 J/m^2 with electron–phonon coupling G_o as 1.4 × 10^{16} W/(m^{3}K).

where G_0 can be considered as the room temperature electron–phonon coupling factor. Eq. (9) is valid under the conditions of $A_{ee0} << B_{ep0}$, T_e, $T_p > T_D$ and $T_e < T_F$ where T_D is the Debye temperature and T_F is the Fermi temperature [23]. T_e and T_p in our measurement range from 300 K to 6000 K, T_D is 170 K, and T_F is 6.39 × 10^4 K for gold, which satisfy these conditions.

Experiment results and discussions

The experiments are carried out on Au-Si samples with different thicknesses of gold (24 nm, 39 nm, 65 nm, and 1 μm (bulk)) and different pump fluences (33.0 J/m^2, 74.3 J/m^2, and 116 J/m^2). In Figure 4, the data of the bulk gold film is shown and is used to find the coupling factor G_0. For these pump fluences, as Figure 4a shows, the coupling between electrons and phonons within the gold film is almost fluence independent. This is because ballistic transport exists in bulk gold. Photo-excited electrons are transferred deep into the material and the temperature rise is lower. The value of G_0 is found to be 1.4 × 10^{16} W/(m^{3}K). This value is similar to that found in [8] (1.5 × 10^{16} W/(m^{3}K)), the difference being that an improved dielectric constant model is used in this work, resulting in an excellent fit to the experimental data for the entire duration of the measurement as seen in Figure 4b. The maximum electron temperatures obtained at these fluences are 463 K, 620 K, and 751 K. These temperatures are relatively low, and thus result in almost the same G according to Eq. (9) and almost the same cooling rates shown in Figure 4a.

Figure 5 shows the measurement data for the 24 nm, 39 nm, and 65 nm thick films, using pump fluences of 33.0, 74.3, and 116 J/m^2. For calculations, G_0 is fixed as 1.4 × 10^{16} W/(m^{3}K), and the interface resistance R_{es} between electrons and the substrate is taken as the fitting parameters to match the experimental data. Phonon-substrate coupling at the interface does not have influence on the measured data over a range of three orders of magnitude [15], and is taken as 1.0 × 10^{-7} m^{2}K/W. It is seen from the figures that when the pump fluence increases,

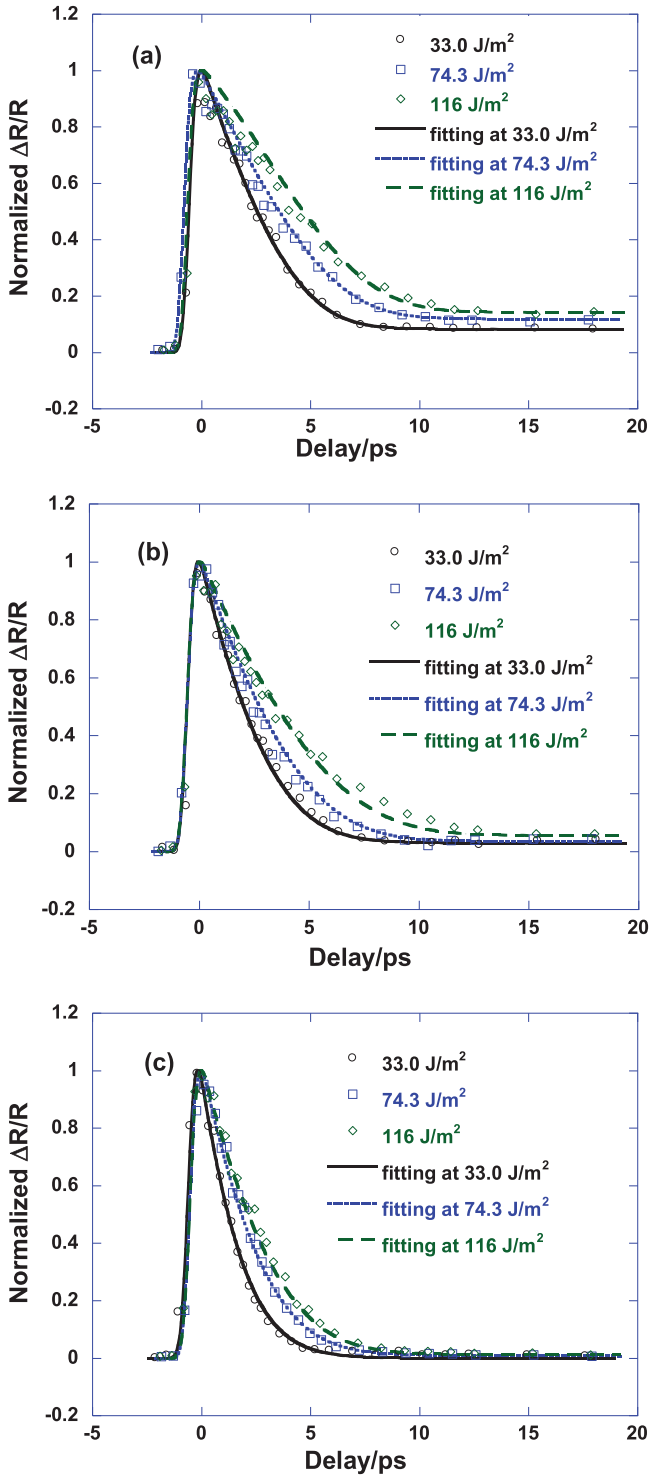

Figure 5. Experiment and fitting result of 24 nm (5a), 39 nm (5b), 65 nm (5c) Au-Si with 490 nm probe and 800 nm pump at 33.0, 74.3, and 116 J/m^2.

the decrease of reflectance is slower. This is because the electron heat capacity C_e increases as the electron temperature increases, which slows down the electron cooling. Comparing the results of different gold films at the same fluence, the thicker gold film has a faster reflectance decrease. This is because in a thick gold film, heat is transported deeper into the film, and the smaller electron heat capacity C_e caused by the lower temperature increases the relaxation rate. It is seen from Figure 5 that agreements are obtained between the calculated optical responses and the experimental data for all the films at all laser fluences.

For the 24 nm-thick film, thermal resistances between electrons in gold and the silicon lattice R_{es} are found to be 2.1×10^{-9} m^{2}K/W, 1.6×10^{-9} m^{2}K/W, and 1.3×10^{-9} m^{2}K/W, for laser fluences of 33.0 J/m^2, 74.3 J/m^2, and 116 J/m^2, which is seen slightly decrease with the increasing fluence. The resistance values are 3.7×10^{-9} m^{2}K/W, 2.9×10^{-9} m^{2}K/W, and 3.0×10^{-9} m^{2}K/W for the 39 nm film, and 3.7×10^{-9} m^{2}K/W, 4.5×10^{-9} m^{2}K/W, and 4.0×10^{-9} m^{2}K/W for the 65 nm film for laser fluences of 33.0 J/m^2, 74.3 J/m^2, and 116 J/m^2.

The uncertainties of interface resistance are estimated, by assuring the experimental noises are within the calculated reflectivity values, using a higher (upper bound) and lower (lower bound) resistance values. The uncertainty values obtained are largely determined by the temperature rise in the gold film. For example, for the 65 nm-thick sample with a laser fluence of 33.0 J/m^2, a relatively low temperature is obtained resulting in a relatively large uncertainty in R_{es}, which is about $\pm$ 13.5% where R_{es} is $(3.7 \pm 0.5) \times 10^{-9}$ m^{2}K/W. For the 24 nm-thick film with a laser fluence of 116 J/cm^2, the uncertainty is reduced to $\pm$ 4.7% where R_{es} is $(2.1 \pm 0.1) \times 10^{-9}$ m^{2}K/W. All the uncertainty values are represented as uncertainty bars in Figure 6.

The inverse of the interface resistance, the interface conductance is assumed to have a similar form of temperature dependence as the electron–phonon coupling G in Eq. (9):

$$h\ (T) = h_0\ \left(C\left(T_e + T_p\right) + 1\right) \tag{10}$$

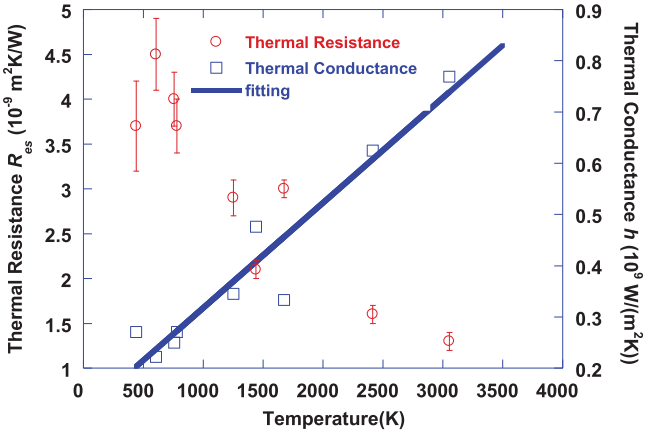

Figure 6. The relationship between interface thermal resistance R_{es}, interface thermal conductance h ($1/R_{es}$), and the maximum electron and phonon temperature T_e+T_p.

h_0 represents the conductance when the electron and phonon temperatures are low. h_0 and C are found from the data in Figure 6 as 1.1×10^8 W/(Km^2), and 1.8×10^{-3} K^{-1}, respectively. It should be noted that the temperatures plotted in Figure 6 and used in Eq. (10) are the maximum electron temperatures and the lattice temperatures at the interface at each laser fluence, while the interface resistance or conductance values were fitted for the time duration when both electron and lattice temperatures are changing. Therefore, the results shown in Figure 6 are only used to provide an estimation of the interface conductance vs. the interface temperature.

The temperature-dependent interface conductance obtained has the same trend as what was reported in [10]. The differences are that h_0 obtained in this work is 1.1×10^8 W/(Km^2) vs. 2.5×10^7 W/(Km^2, C is 1.8×10^{-3} K^{-1} vs. 1.4×10^{-2} K^{-1}, and the temperature coefficient $h_0 \times C$ is 2.1×10^5 W/ (m^{2}K^2) vs. 3.5×10^5 W/ (m^{2}K^2). Therefore, the results obtained in this work have a higher low-temperature thermal conductance and are less temperature-dependent. The samples used in the two studies may not be identical. In addition, it is noted that 800 nm pump and probe beams were used in [10]. As discussed earlier, probing with energy near ITT significantly reduces the effect of non-thermalized electrons. Also, we determined electron–phonon coupling factor G_0 from bulk gold which was then used in the determination of thermal conductance at the interface. We noted that many related works obtained a higher G value for electron–phonon coupling in gold and considering G as a temperature independent factor, for example, 2.9×10^{16} W/(m^{3}K) with an 800 nm probe in [24], 2.7×10^{16} W/(m^{3}K) with a 630 nm probe in [25], 4.0×10^{16} W/(m^{3}K) with a 615 nm probe in [3], and 2.2×10^{16} W/(m^{3}K) with a 785 nm probe in [26]. Because these probe wavelengths are farther from ITT, the states probed can be much affected by the non-thermalized electrons as shown in Figure 2 and the non-thermalized states tend to disappear faster than the coupling process between electrons and the lattice.

The result of h_o represents the low-temperature limit of the interface conductance between electrons in metal and the dielectric substrate. In this work, it was found to be about 1.1×10^8 W/(Km^2) at the gold–silicon interface. There have been a great deal of works for quantifying the conductance at the metal-dielectric interface but in general a total conductance including contributions from both electron-substrate and phonon (in metal)-substrate coupling is obtained [e.g., 27]. Moreover, it was often assumed that the electron-substrate contribution to the total interface conductance is small. Our work shows that the electron-substrate conductance is of the same order of the total conductance reported in literature, and it is possible to independently quantify this electron-substrate conductance.

Conclusions

Heat transfer at the metal-dielectric interface is a major concern in ultrafast spectroscopy with the pump-probe technique. In many previous works, the probe energy chosen for detecting the transient reflectance change was far from ITT in metal (gold), and the signals detected tended to be influenced by non-thermalized electrons and overestimated both the electron–phonon coupling rate within the metal film and the electron–phonon thermal conductance at the metal-dielectric interface. In this work, measurements were carried out using the 490 nm probe, near ITT of gold to reduce the effect of non-thermalized electrons and also increase the measurement sensitivity. We also introduced a temperature-dependent Drude–Lorentz model for the dielectric constant of gold. Combined with the two-temperature model, it provided an excellent agreement with the experimental data. Our results showed that the interface conductance increased linearly with the interface temperature within the laser fluence range used in this work. This allows for extrapolation of the interface conductance between electrons in metal and the substrate to near the room temperature, which is of importance for quantifying interface conductance in details. In addition, our method can be extended for the study of other metal-dielectric systems of interest in the future.

Nomenclature

A_{ee}	electron-electron scattering coefficient, s^{-1}.K^{-2}
B_{ep}	electron–phonon scattering coefficient, s^{-1}.K^{-1}
C	volumetric heat capacity, J.m^{-3}.K^{-1}
D_i	Lorentz oscillator amplitude, s^{-1}
E	energy, eV
E_f	Fermi energy, eV
EO	electron occupation
f	Fermi function
G	electron–phonon coupling factor, W.m^{-3}.K^{-1}
G_0	bulk electron–phonon coupling factor, W.m^{-3}.K^{-1}
h	interface conductance, W.K^{-1}m^{-2}
h_0	room temp thermal conductance, W.K^{-1}.m^{-1}
ITT	interband transition threshold, eV
J	pump fluence, W.m^{-2}
k	thermal conductivity, W.m^{-1}.K^{-1}
k_B	Boltzmann constant, m^2.kg.K^{-1}.s^{-2}
L	thickness of gold film, m
L_i	Lorentz oscillator terms
OPA	optical parametric amplifier
R	reflection coefficient

R_{es}	electron substrate interface resistance, $m^2.K.W^{-1}$
R_{ps}	phonon substrate interface resistance, $m^2.K.W^{-1}$
S	volumetric heat generation, $W.m^{-3}$
t	time, s
T	temperature, K
T_0	room temperature, K
T_F	Fermi temperature, K
T_D	Debye temperature, K
t_p	pulse duration, s
TTM	two temperature model
x	x coordinate, m
Y_i	temperature independent scattering coefficient, s^{-1}

Greek symbols

ε	dielectric constant
ε_1	real part of dielectric constant
ε_2	imaginary part of dielectric constant
ε_∞	high frequency permittivity
δ	optical penetration depth, m
δ_b	electron ballistic length, m
ϕ_i	Lorentz oscillator phase, rad
Γ_0	Drude damping term, $rad.s^{-1}$
Γ_i	Lorentz damping term, $rad.s^{-1}$
μ_i	order of pole
ω	frequency, $rad.s^{-1}$
ω_p	plasmon frequency, $rad.s^{-1}$
ω_i	Lorentz oscillator resonant frequency, $rad.s^{-1}$

Subscripts

e	electron
p	phonon
s	substrate
0	Drude term
1	first Lorentz oscillator term
2	second Lorentz oscillator term

Acknowledgments

This work is supported in part by DARPA MESO (grant number N66001-11-1-4107) and the department of Energy (Award No. DE-EE0005432) through the General Motors. We also thank Dr. Xiulin Ruan of the School of Mechanical Engineering, Purdue University for valuable discussions.

Funding

This work is supported in part by DARPA MESO (grant number N66001-11-1-4107), the department of Energy (Award No. DE-EE0005432) through the General Motors, and the National Science Foundation (Award No. 1462622-CMMI).

Notes on contributors

Qiaomu Yao received his Bachelor's degree in Mechanical Engineering at Xi'an Jiaotong University in 2013, and finished his Master degree in Mechanical Engineering and Computer Engineering at Purdue University at 2015. He worked in Prof. Xianfan Xu's group on the project about Au-Si interface heat transfer on the nanoscale with ultrafast laser during his study at Purdue University from 2013 to 2015.

Liang Guo received his Bachelor's degree in Mechanical Engineering at Tsinghua University in 2009. He conducted graduate research on nanoscale heat transfer in Prof. Xianfan Xu's group in Mechanical Engineering, Purdue University. His projects include heat transfer across metal-dielectric interfaces, wavelength tuning effect in TDTR, and phonon dynamics in thermoelectrics based on Bi_2Te_3 and skutterudites. He obtained his Ph.D degree in 2014, after which he utilized femtosecond four-wave mixing (FWM including two-pulse photo echo, three-pulse photo echo and 2DES) to study energy transfer in novel semiconductors in Prof. Graham Fleming's group in Chemistry, University of California, Berkeley. His current project is on exciton dynamics in monolayer transition metal dichalcogenides (TMDCs).

Vasudevan Iyer received his Bachelor's degree in Mechanical Engineering from Indian Institute of Technology Madras in 2014. He is currently pursuing his PhD degree at Purdue University in Professor Xianfan Xu's group. His research interests include optical techniques using ultrafast lasers to study heat and electronic transport in metals and semiconductors.

Xianfan Xu is the James J. and Carol L. Shuttleworth Professor of Mechanical Engineering at Purdue University. He received B.Eng. in Engineering Thermophysics from the University of Science and Technology of China in 1989, and M.S. and Ph.D. in Mechanical Engineering from the University of California, Berkeley in 1991 and 1994. His current research is focused on heat transfer in nanoscale

materials, heat transfer in micro and nanoscale materials processing and manufacturing, fundamentals of nanoscale radiation, and applications in nanoscale materials processing and manufacturing. He has written about 400 publications, including over 170 archival journal papers, 6 book chapters, and many conference papers and technical reports, and has given over 100 invited talks. He is a Fellow of ASME and a Fellow of SPIE – the International Society for Optics and Photonics. He received the ASME Heat Transfer Memorial Award in 2014.

References

[1] J. Hohlfeld et al., "Electron and lattice dynamics following optical excitation of metals," *Chem. Phys.*, vol. 251, no. 1, pp. 237–258, Jan. 2000. doi:10.1016/S0301-0104(99)00330-4.

[2] T. Hatakeyama and K. Fushinobu, "Electro-thermal behavior of a sub-micrometer bulk CMOS device: modeling of heat generation and prediction of temperatures," *Heat Transf. Eng.*, vol. 29, no. 2, pp. 120–133, Feb. 2008. doi:10.1080/01457630701673162.

[3] H. E. Elsayed-Ali, T. Juhasz, G. O. Smith, and W. E. Bron, "Femtosecond thermoreflectivity and thermotransmissivity of polycrystalline and single-crystalline gold films," *Phys. Rev. B*, vol. 43, no. 5, pp. 4488–4491, Feb. 1991. doi:10.1103/PhysRevB.43.4488.

[4] W. S. Fann, R. Storz, H. W. K. Tom, and J. Bokor, "Direct measurement of nonequilibrium electron-energy distributions in subpicosecond laser-heated gold films," *Phys. Rev. Lett.*, vol. 68, no. 18, pp. 2834–2837, May. 1992. doi:10.1103/PhysRevLett.68.2834.

[5] A. N. Smith and P. M. Norris, "Influence of intraband transitions on the electron thermoreflectance response of metals," *Appl. Phys. Lett.*, vol. 78, no. 9, pp. 1240–1242, Feb. 2001. doi:10.1063/1.1351523.

[6] C. Kittel, *Introduction to Solid State Physics*. New York, NY, USA: John Wiley & Sons, Inc., 1976.

[7] C. K. Sun, F. Vallée, L. H. Acioli, E. P. Ippen, and J. G. Fujimoto, "Femtosecond-tunable measurement of electron thermalization in gold," *Phys. Rev. B*, vol. 50, no. 20, pp. 15337–15348, Nov. 1994. doi:10.1103/PhysRevB.50.15337.

[8] L. Guo and X. Xu, "Ultrafast spectroscopy of electron-phonon coupling in gold," *ASME J. Heat Transf.*, vol. 136, no. 12, pp. 122401-122401-6, Sept. 2014. doi:10.1115/1.4028543.

[9] A. Giri, J. T. Gaskins, B. M. Foley, R. Cheaito, and P. E. Hopkins, "Experimental evidence of excited electron number density and temperature effects on electron-phonon coupling in gold films," *J. Appl. Phys.*, vol. 117, no. 4, pp. 044305 (8 pages), Jan. 2015. doi:10.1063/1.4906553.

[10] P. E. Hopkins, J. L. Kassebaum, and P. M. Norris, "Effects of electron scattering at metal–nonmetal interfaces on electron-phonon equilibration in gold films," *J. Appl. Phys.*, vol. 105, no. 2, pp. 023710 (8 pages), Jan. 2009. doi:10.1063/1.3068476.

[11] N. Del Fatti et al., "Nonequilibrium electron dynamics in noble metals," *Phys. Rev. B*, vol. 61, no. 24, pp. 16956–16966, Jan. 2000. doi:10.1103/PhysRevB.61.16956.

[12] S. I. Anisimov, B. L. Kapeliovich, and T. L. Perel'man, "Electron emission from metal surfaces exposed to ultrashort laser pulses," *Sov. Phys. JETP*, vol. 39, no. 2, pp. 375–377, Aug. 1974.

[13] T. Q. Qiu and C. L. Tien, "Heat transfer mechanisms during short-pulse laser heating of metals," *ASME J. Heat Transf.*, vol. 115, no. 4, pp. 835–841, Nov. 1993. doi:10.1115/1.2911377.

[14] A. Khadrawi and M. Al-Nimr, "Microscopic vs. macroscopic hyperbolic heat conduction: validation criterion under the effect of a moving heating source," *Heat Transfer Eng.*, vol. 26, no. 10, pp. 73–79, Oct. 2005. doi:10.1080/01457630500248703.

[15] L. Guo, S. L. Hodson, T. S. Fisher, and X. Xu, "Heat transfer across metal-dielectric interfaces during ultrafast-laser heating," *ASME J. Heat Transf.*, vol. 134, no. 4, pp. 042402-042402-5, Feb. 2012. doi:10.1115/1.4005255.

[16] I. H. Chowdhury and X. Xu, "Heat transfer in femtosecond laser processing of metal," *Numer. Heat Transf., Part A*, vol. 44, no. 3, pp. 219–232, Mar. 2003. doi:10.1080/716100504.

[17] P. G. Etchegoin, E. C. Le Ru, and M. Meyer, "An analytic model for the optical properties of gold," *J. Chem. Phys*, vol. 125, no. 16, pp. 164705 (3 pages), Oct. 2006. doi:10.1063/1.2360270.

[18] D. Barchiesi and T. Grosges, "Fitting the optical constants of gold, silver, chromium, titanium, and aluminum in the visible bandwidth," *J. Nanophoton.*, vol. 8, no. 1, pp. 083097 (16 pages), Jan. 2014. doi:10.1117/1.JNP.8.083097.

[19] N. W. Ashcroft and N. D. Mermin, *Solid State Physics*. Philadelphia, PA, USA: W. B. Saunders, 1976.

[20] A. H. MacDonald, "Electron-Phonon enhancement of electron-electron scattering in Al," *Phys. Rev. Lett.*, vol. 44, no. 7, pp. 489–493, Feb. 1980. doi:10.1103/PhysRevLett.44.489.

[21] P. B. Johnson, and R. W. Christy, "Optical constants of the noble metals," *Phys. Rev. B*, vol. 6, no. 12, pp. 4370–4379, Dec. 1972. doi:10.1103/PhysRevB.6.4370.

[22] F. L. Pedrotti, L. S. Pedrotti, and L. M. Pedrotti, *Introduction to Optics*. Upper Saddle River, NJ, USA: Pearson Prentice Hall, 2007.

[23] J. K. Chen, W. P. Latham, and J. E. Beraun, "The role of electron–phonon coupling in ultrafast laser heating," *J. Laser Appl.*, vol. 17, no. 1, pp. 63–68, Feb. 2005. doi:10.2351/1.1848522.

[24] J. L. Hostetler, A. N. Smith, D. M. Czajkowsky, and P. M. Norris, "Measurement of the electron-phonon coupling factor dependence on film thickness and grain size in Au, Cr, and Al," *Appl. Opt.*, vol. 38, no. 16, pp. 3614–3620, Jan. 1999. doi:10.1364/AO.38.003614.

[25] S. D. Brorson et al., "Femtosecond room-temperature measurement of the electron-phonon coupling constant λ in metallic superconductors," *Phys. Rev. Lett.*, vol. 64, no. 18, pp. 2172–2175, Apr. 1990. doi:10.1103/PhysRevLett.64.2172.

[26] G.-M. Choi, R. B. Wilson, and D. G. Cahill, "Indirect heating of Pt by short-pulse laser irradiation of Au in a Nanoscale Pt/Au Bilayer," *Phys. Rev. B*, vol. 89, no. 6, pp. 064307 (7 pages), Jan. 2014. doi:10.1103/PhysRevB.89.064307.

[27] H.-K. Lyeo and D. G. Cahill, "Thermal conductance of interfaces between highly dissimilar materials," *Phys. Rev. B*, vol. 73, no. 14, pp. 144301 (6 pages), Apr. 2006. doi:10.1103/PhysRevB.73.144301.